X-ray fluorescence of layered synthetic materials with interfacial roughness

A. Król, C. J. Sher, and Y. H. Kao

Department of Physics, State University of New York at Stony Brook, Stony Brook, New York 11794-3800

(Received 26 April 1988)

Measurements of x-ray fluorescence versus grazing incidence angle at fixed incoming photon energy can provide useful information on surface and interfacial microstructure. A matrix formulation suitable for analysis of radiant energy flow inside a layered material, and hence angular fluorescence emission, is presented, and a vector scattering model is employed to account for the effect of interfacial roughness. Good agreement between experimental results of x-ray fluorescence yield and the model calculations has been obtained in a semiconductor heterostructure and a superlattice system.

I. INTRODUCTION

Recently there has been considerable interest in the study of various types of layered synthetic materials. Successful preparation of quantum well structures and heterojunctions by epitaxial growth has led to significant progress in the fundamental understanding of two-dimensional electron systems, and also the advent of a new semiconductor technology. Despite extensive work in the past on the physical and structural properties of layered systems, a fundamental barrier to a more efficient use of these new synthetic materials in optical and electronic devices has been the lack of understanding of microscopic structures in the vicinity of interfaces and impurity atoms. Innovative approaches to microscopic probing, especially nondestructive characterization, of microstructures in layered synthetic materials (LSM's) would seem highly desirable.

X-ray fluorescence measurement offers an important advantage for probing the microstructures due to its element selectivity. The fluorescence yield (FY) resulting from a given atomic species is determined by the depth profile of the atoms and the variation of energy flow in the material. Hence, by measuring the FY as a function of the field distribution, which can be controlled by varying the grazing incidence angle, the atomic profile of a given species in a complex material system can be selectively probed.

The presence of interfaces in heterojunctions and superlattices gives rise to a mismatch of the optical constants between adjacent layered materials. The field is different from that in the bulk, depending on the properties of the constituent materials and the microstructure of the interfaces. The FY measurements can therefore provide information on the optical constants and thickness of the layers, as well as the interfacial roughness in LSM. Since the fluorescence energies of different atomic species are usually well separated, the effect on interfacial roughness due to different constituent atoms can also be investigated by this element-selective technique.

In the present work we introduce a matrix formulation of the energy flow, which is applied to the analysis of FY from layered materials. Our connection formula for calculating the electric and magnetic field intensity at any depth inside a LSM takes into account the effect of uncorrelated surface and interfacial roughness by means of a vector scattering model. Although the x-ray FY technique has been used in the past for studying LSM's, this method for quantitative analysis of FY and interfacial roughness in layered materials has hitherto not been found in the literature.

A brief review of previous work is given in Sec. II. Our model of using a matrix formulation for calculating the energy flow in a LSM and for analyzing the FY in a LSM with interfacial roughness is presented in Secs. III and IV, including a consideration of the different cases of s and p polarization of the x rays. By way of examples, this model is then used to compute the FY of two different LSM systems in which very good agreement with the experimental results has been achieved. This comparison is given in Sec. V.

II. BACKGROUND

There exist two approaches to the problem of x-ray interaction with finite multilayered systems. The first one is based on the dynamical theory of Darvin-Princ and Ewald,[1−6] and the second is based on the optical electromagnetic wave solution of the Fresnel equation (OEMF) on each interface.[7,8] Hanke et al.[6] have recently demonstrated the equivalence of both methods.

Electromagnetic wave propagation in a layered structure in the visible regime has been the subject of investigations for many years, starting with the pioneering work of Airy in 1833.[9] A review of the early papers on this topic can be found in Born and Wolf[7] and Berning.[8] The problem of x-ray propagation in a stratified media was considered for the first time by Kiessing[10] and then by Parratt.[11] They observed grazing-angle specular reflectivity on stratified absorbing media and described this phenomenon in the framework of the OEMF theory.

Although many different types of "imperfections" may exist in a LSM, for example interfacial roughness, compositional variations, bulk inhomogeneities, and compositionally graded interfaces (see the discussion in Ref. 12), there exists a common belief that the predominant factor which deteriorates the device performance of LSM's is surface and interfacial roughness. In the grazing in-

cidence angle regime, roughness can be regarded as un-correlated since the radiation covers a large distance in the lateral direction between interfaces.[13] For this reason we will focus our attention mainly on the roughness "imperfection" in the proposed model of fluorescence emission from LSM's.

In 1974 Eastman[14] extended the classical scalar treatment of surface roughness by Beckmann and Spizzichino[15] (see also bibliography given by Elson and Bennett[16]) to uncorrelated interfacial roughness in stratified media in the visible region. In 1979 Carniglia[17] incorporated additive interfacial roughness and uncorrelated bulk inhomogeneities to this theory. At the same time a vector model of light scattering on multilayer dielectric mirrors with rough interfaces was developed by Elson and co-workers[18] and independently by Croce.[19] In 1980 this method was used by Névot and Croce[20] to describe the grazing-angle reflectivity of multilayer structures in the x-ray regime. In the same year Bousquet *et al.*[21] proposed a vector theory for calculating scattered radiant energy in any direction; however, this method requires a knowledge of the autocorrelation and cross correlation function on each interface. More recently Vidal and Vincent,[22] using a generalized reciprocity relation,[23] have presented a new vector method describing specularly reflected and transmitted x rays in LSM's with uncorrelated interfacial roughness.

One can distinguish two different phenomena pertinent to grazing incidence: evanescent-wave effects (below the critical angle) and standing-wave effects (above the critical angle). Standing-wave fluorescence (SWF) from crystal surfaces has been investigated for many years.[24–35] However, evanescent-wave fluorescence (EWF) has only recently become the subject of experimental studies on crystal surfaces[36–38] and liquids.[39] The first EWF and SWF experiment on a LSM was performed by Barbee and Warburton[40,41] in 1984. In the subsequent years several reports about angular FY in multilayer structures were published.[42–44]

It has been proven that angular FY in the grazing-angle regime can provide very precise information on the atomic structure of the surface or interfaces. Due to its element sensitivity this method is very well suited to obtain the position and distribution of impurity atoms within the material or adsorbed atoms on surfaces. FY can also be employed in order to obtain optical constants, layer thicknesses, and other parameters which are needed to describe the LSM's.

It appears that evanescent- and standing-wave fluorescence from multilayer systems is a promising new technique which is moving forward rapidly and will have many potential applications in fundamental research as well as in some practical areas.

In the present work, the angular x-ray fluorescence yield from stratified media is calculated and the influence of surface and interfacial roughness is studied; these results are compared with some experimental data.

III. GENERAL DESCRIPTION OF THE MODEL

In the proposed model of fluorescence yield from LSM's in the grazing incidence regime, we utilize the

OEMF matrix theory of x-ray interaction with stratified media, incorporating Vidal and Vincent's vector model of radiation scattering on uncorrelated interfacial roughness. We consider a stratified material system shown in Fig. 1. Each layer is characterized by a complex refractive index obtained from the quantum theory of dispersion,[1,2] assuming that the permeability constant is unity for x rays. The refractive index for the *j*th layer has the form

$$\hat{n}_j = 1 - \delta_j + i\beta_j \ . \tag{1}$$

The first medium is vacuum (or air) with $\delta_0, \beta_0 = 0$.

We also assume that all "imperfections" can be described in terms of surface or interfacial uncorrelated roughness, which is a reasonable approximation for grazing-angle incidence of x rays in LSM's grown by molecular-beam epitaxy (MBE).[12,13] In order to describe the x-ray interaction with a layered system, we will employ the OEMF theory in its matrix representation, modified by the introduction of characteristic scattering matrices. These matrices are obtained from the vector scattering theory proposed by Vidal and Vincent,[22] and they describe specular scattering on rough interfaces with uncorrelated roughnesses. Diffuse scattering will be neglected as it is generally known to be 2 or 3 orders of magnitude weaker than specular scattering,[18] although for extremely small $(\theta/\theta_C \ll 1)$ and extremely large $[R(\theta) \ll 10^{-5}]$ grazing angles diffuse scattering can be comparable with specular scattering.[45] The notation used in the present paper is shown in Fig. 1.

IV. ELECTRIC AND MAGNETIC FIELD AND ENERGY FLOW IN LSM WITH ROUGH INTERFACES

A. *s* polarization

Let us consider an interface *j* between two homogeneous media (see Fig. 1). In medium *j*, which is located above the *j*th interface, the total electric field, polarized perpendicular to the plane of incidence, can be decomposed into two components: transmitted field E_j^+ and reflected field E_j^-.[7,8] The total electric field in the *j*th layer can be written as follows:

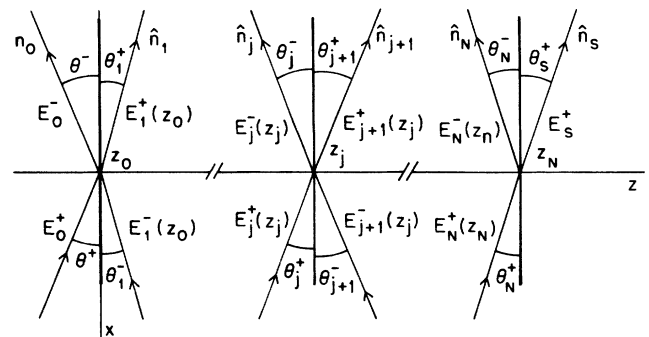$$E_j(\mathbf{r}) = E_j^+(\mathbf{r}) + E_j^-(\mathbf{r}) \tag{2}$$

FIG. 1. Schematic representation of reflection and refraction for stratified homogeneous media.

where (see the Appendix)

$$E_j^+(\mathbf{r}) = \hat{A}_j \exp(i\hat{p}_j z)\exp(ik_{0x}x) \; , \tag{3a}$$

$$E_j^-(\mathbf{r}) = \hat{B}_j \exp(-i\hat{p}_j z)\exp(ik_{0x}x) \; , \tag{3b}$$

$$k_{jx} = k_j\cos\theta_j = k_{j+1}\cos\theta_{j+1} = k_{j+1x} = k_{0x} \; , \tag{3c}$$

$$\hat{p}_j = k_j\sin\theta_j + ia_j = (k_0^2\hat{n}_j^2 - k_0^2 n_0^2\cos^2\theta)^{1/2} \; . \tag{3d}$$

θ_j will be referred to as the refraction angle in the medium j. The notation $\hat{p}_j$ is introduced to emphasize that $\hat{p}_j$ is a complex quantity.

At this point we would like to emphasize that the electric field in a LSM is an inhomogeneous plane wave[46,47] with a complex wave vector $\hat{\mathbf{k}}_j$ and an attenuation vector $\mathbf{a}_j$ perpendicular to interfaces; i.e., planes of constant amplitude are parallel to boundaries.

$$
\begin{bmatrix} E_{j+1}^+(z_j) \\ E_{j+1}^-(z_j) \end{bmatrix} = \begin{bmatrix} \exp[-i\hat{p}_{j+1}(z-z_j)] & 0 \\ 0 & \exp[i\hat{p}_{j+1}(z-z_j)] \end{bmatrix} \begin{bmatrix} E_{j+1}^+(z) \\ E_{j+1}^-(z) \end{bmatrix}
$$

$$
= \tilde{T}_{j+1}(z-z_j)\begin{bmatrix} E_{j+1}^+(z) \\ E_{j+1}^-(z) \end{bmatrix} \; . \tag{5}
$$

We now take into account the influence of a rough interface [with a mean plane parallel to the (xy) plane] on the electric field in the medium. According to Ref. 22, after some transformation, one can obtain the following scattering matrix $\tilde{S}_j$ describing the influence of a rough jth interface on the field (assuming a normal distribution of the deviation from the mean plane in the real interface):

$$
\tilde{S}_j = \frac{1}{1-\hat{r}_j^2}\begin{bmatrix} \hat{e}_j^- - \hat{r}_j^2\hat{e}_j^+ & \hat{r}_j(\hat{e}_j^+ - \hat{e}_j^-) \\ \hat{r}_j(\hat{e}_j^+ - \hat{e}_j^-) & \hat{e}_j^- - \hat{r}_j^2\hat{e}_j^+ \end{bmatrix} \tag{6}
$$

where

$$\hat{e}_j^+ = \exp[-(\hat{p}_{j+1}+\hat{p}_j)^2\sigma_j^2/2] \; , \tag{7a}$$

$$\hat{e}_j^- = \exp[-(\hat{p}_{j+1}-\hat{p}_j)^2\sigma_j^2/2] \; . \tag{7b}$$

σ_j is the rms roughness parameter of the jth interface. The roughness description presented here is valid for any σ/λ ratio but not in a region where surface plasmons are present.

Using (4), (5), and (6) we can write a connection formula describing the electric field rearrangement along the z axis:

$$
\begin{bmatrix} E_j^+(z_j) \\ E_j^-(z_j) \end{bmatrix} = \tilde{I}_j\tilde{S}_j\tilde{T}_{j+1}(z-z_j)\begin{bmatrix} E_{j+1}^+(z) \\ E_{j+1}^-(z) \end{bmatrix} \; . \tag{8}
$$

It is interesting to note that in our model the electric field due to a rough interface now has a discontinuity at the interface (cf. Refs. 18 and 22).

In the substrate where no reflection occurs, we can define a $\tilde{P}_{0N}$ matrix to relate the field at the substrate E_S^+ to that at the top surface (see Fig. 1):

Following the OEMF method we can find the matrix $\tilde{I}_j$ which connects the electric field components below and above the jth interface:

$$
\begin{bmatrix} E_j^+(z_j) \\ E_j^-(z_j) \end{bmatrix} = \frac{1}{\hat{t}_j}\begin{bmatrix} 1 & \hat{r}_j \\ \hat{r}_j & 1 \end{bmatrix}\begin{bmatrix} E_{j+1}^+(z_j) \\ E_{j+1}^-(z_j) \end{bmatrix}
$$

$$
= \tilde{I}_j\begin{bmatrix} E_{j+1}^+(z_j) \\ E_{j+1}^-(z_j) \end{bmatrix} \tag{4}
$$

where $\hat{r}_j$ and $\hat{t}_j$ are the Fresnel coefficients for s polarization.

The matrix $\tilde{T}_{j+1}(z-z_j)$ describing the connection between the electric field at point z_j on the jth interface and that at some point z $(z_j < z < z_{j+1})$ within the $(j+1)$th layer can be written in the form

$$\tilde{P}_{0N} = \tilde{I}_0\tilde{S}_0\tilde{T}_1(z_1-z_0)\tilde{I}_1\tilde{S}_1\tilde{T}_2(z_2-z_1)\cdots\tilde{I}_N\tilde{S}_N \tag{9a}$$

where

$$
\tilde{P}_{0N} = \begin{bmatrix} p_{11}^{0N} & p_{12}^{0N} \\ p_{21}^{0N} & p_{22}^{0N} \end{bmatrix} \tag{9b}
$$

and finally

$$
\begin{bmatrix} E_0^+(z_0) \\ E_0^-(z_0) \end{bmatrix} = \tilde{P}_{0N}\begin{bmatrix} E_S^+(z_N) \\ 0 \end{bmatrix} \; . \tag{9c}
$$

Now we can find the electric field at any point z in the LSM for $z_{j-1} < z < z_j$ using the $\tilde{P}_{jN}$ matrix defined in the following:

$$\tilde{P}_{jN} = \tilde{I}_j\tilde{S}_j\tilde{T}_{j+1}(z_{j+1}-z_j)\cdots\tilde{I}_N\tilde{S}_N \tag{10a}$$

based on the fact that

$$
\begin{bmatrix} E_j^+(z) \\ E_j^-(z) \end{bmatrix} = \tilde{T}_j(z_j-z)\tilde{P}_{jN}\begin{bmatrix} E_S^+(z_N) \\ 0 \end{bmatrix} \; . \tag{10b}
$$

The electric field $E_S^+(z_N)$ in the substrate, below the Nth interface, can be found from (9c):

$$E_S^+(\theta,z_N) = \frac{E_0^+(z_0)}{p_{11}^{0N}} = \frac{E_i}{p_{11}^{0N}} \tag{11}$$

where E_i is the amplitude of the incoming x rays with s polarization. After substitution of (5), (10b), and (11) into (2) the total electric field at any point z $(z_{j-1} < z < z_j)$ can be written in the form

$$E_j(\theta,z) = \{p_{11}^{jN}\exp[i\hat{p}_j(z_j - z)]$$

$$+ p_{21}^{jN}\exp[-i\hat{p}_j(z_j - z)]\}E_i / p_{11}^{0N}$$

$$= E_y(\theta,z) .$$ (12)

For $z > z_N$ (i.e., in the substrate) one can obtain

$$E_S(\theta,z) = E_{N+1}^+(z)$$

$$= \exp[i\hat{p}_S(z - z_N)]E_i / p_{11}^{0N} = E_y(\theta,z) .$$ (13)

The magnetic field can be found from Maxwell's equations for any point z ($z_{j+1} < z < z_j$ and $\mu_j = 1$):

$$H_{jx}(\theta,z) = \hat{p}_j(\theta)[E_j^-(\theta,z) - E_j^+(\theta,z)]/k_0 ,$$ (14a)

$$H_{jy} = 0 ,$$ (14b)

$$H_{jz}(\theta,z) = k_{0x}(\theta)[E_j^-(\theta,z) + E_j^+(\theta,z)]/k_0 .$$ (14c)

The time average of the density of radiant energy flow, i.e., the Poynting vector $\mathbf{P}(\theta,z)$, can be obtained from the following formula:[48]

$$\mathbf{P}(\theta,z) = \text{Re}(\mathbf{S}) = C\langle \text{Re}(\mathbf{E} \times \mathbf{H}^*)\rangle$$ (15)

where Re means the real part, $\langle \ \rangle$ the time average, and C is a multiplicative constant. In terms of components we have

$$P_x(\theta,z) = \text{Re}(S_x) = C\langle \text{Re}[E_y(\theta,z)H_z(\theta,z)^*]\rangle ,$$ (16a)

$$P_y = 0 ,$$ (16b)

$$P_z(\theta,z) = \text{Re}(S_z) = -C\langle \text{Re}[E_y(\theta,z)H_x(\theta,z)^*]\rangle ,$$ (16c)

where $E_y(\theta,z)$ is defined by (12) or (13). After some manipulation one can obtain

$$P_{jx}(\theta,z) = Cn_0\cos\{ |E_j^+|^2 + |E_j^-|^2$$

$$+ 2|E_j^+| \ |E_j^-|\cos[(2k_j\sin\theta_j)z$$

$$+ \alpha_j - \beta_j]\} ,$$ (17a)

$$P_{jz}(\theta,z) = (C/k_0)\{k_j\sin\theta_j(|E_j^+|^2 - |E_j^-|^2)$$

$$- 2|E_j^+| \ |E_j^-| a_j\sin[(2k_j\sin\theta_j)z$$

$$+ \alpha_j - \beta_j]\} .$$ (17b)

In the substrate, i.e., $z_N < z$:

$$P_{Sx}(\theta,z) = C\cos\theta | E_S^+|^2 ,$$ (18a)

$$P_{Sz}(\theta,z) = Ck_S\sin\theta | E_S^+|^2/k_0 ,$$ (18b)

where subscript S refers to the substrate. It can be seen that energy flows in the plane of incidence. We would like to emphasize that the planes of constant energy flow lie parallel to the interfaces, in agreement with our earlier results that the planes of constant amplitude of the electric and magnetic fields are parallel to the interfaces. The normal component of density of energy flow (17b) is proportional to the difference between normal components of the Poynting vector of transmitted and reflected waves, as expected, but also contains a cross product term which

is proportional to the magnitude of the attenuation vector. Due to this term one should expect the appearance of interference effects between the transmitted and reflected waves in an absorbing medium. The tangential component of the density of radiant flux (17a) is proportional to the sum of transmitted and reflected fluxes plus a cross product. Interference effects for this component are always expected (even for a nonabsorbing medium) for oblique incidence.

The critical angle for a LSM is defined as the grazing angle at which the specular reflectivity reaches half of its maximum value, or the inflection point.[12] For a heterostructure, this can be estimated to be $\sqrt{2\delta}$.[10,11]

As an example, we consider the simplest LSM, i.e., a heterojunction consisting of a thin layer on a substrate. The dependence of the magnitude of the z component of the Poynting vector is shown in Fig. 2 for a ZnSe/GaAs heterostructure with a 200-Å ZnSe layer on a GaAs substrate. As expected, for an incidence angle of 2 mrad, which is below the critical angle [see Fig. 2(a)], P_z decreases rapidly with z. At 30 Å below the surface P_z is very small, which can be compared with the penetration depth. For an incidence angle equal to the critical angle θ_C [see Fig. 2(b)] the radiation is present in the entire structure. For $\theta > \theta_C$ [see Fig. 2(c)] energy can be effectively transmitted into the substrate and one can ob-
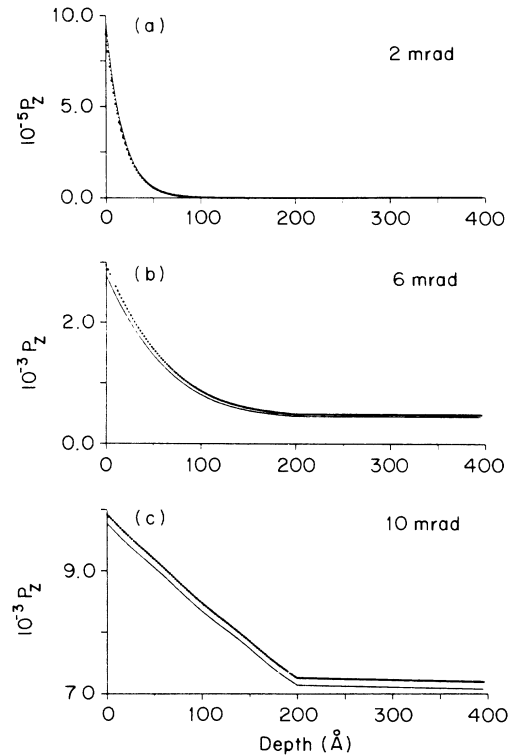

FIG. 2. Calculated magnitude of the normal (z) component of the normalized Poynting vector vs depth in a ZnSe(200 Å)/GaAs heterostructure shown at 2, 6, and 10 mrad grazing angle, for 9.7 keV energy of incoming photons with s polarization. The solid line represents the result obtained for a heterostructure with no roughness; the dotted line represents the result obtained for a heterostructure with 10 Å of rms roughness.

serve weak oscillations of $P_z(\theta)$. Under this condition, the effect of rough interfaces leads to a slight enhancement of the magnitude of this component.

The density of energy flow parallel to the interfaces is shown in Fig. 3 for the same heterostructure as in Fig. 2. The primary difference in the behavior of this component versus the normal component is that now we do observe strong oscillations of its magnitude for large angles of incidence [see Fig. 3(c)]. Let us also note that the tangential component is much stronger than the normal component due to grazing angle of incidence. We do observe a jump of the energy flow at the rough interface. This is a consequence of our model of scattering.

The magnitude of the density of energy flow normalized to the incoming beam intensity inside the thin layer of ZnSe on GaAs is shown in Fig. 4. For $z=2$ Å, i.e., very close to surface [see Fig. 4(a)], the Poynting vector vanishes only for $\theta=0$ and gradually reaches its maximum at the critical angle. For higher angles it decreases with pronounced oscillations, displaying increasing period and decaying amplitude. At $z=100$ and 198 Å [see Figs. 4(b) and 4(c)], i.e., in the midpoint of the ZnSe layer and very close to the interface, respectively, the Poynting vector vanishes for subcritical incidence angles, as is expected from the penetration depth estimation for
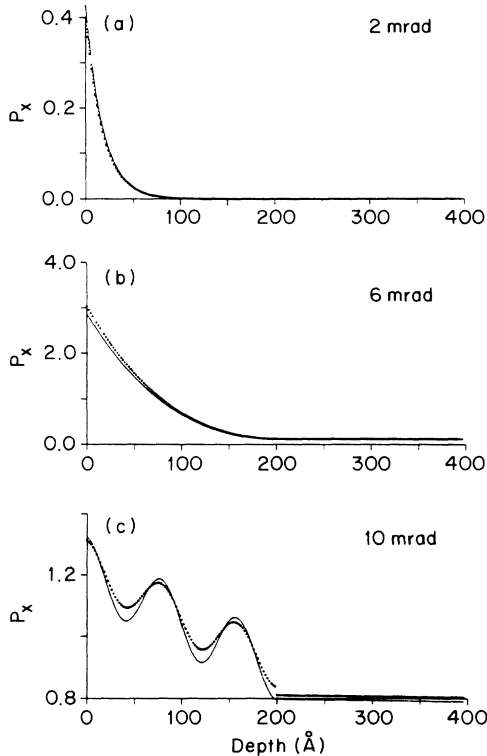
FIG. 3. Calculated magnitude of the tangential (x) component of the normalized Poynting vector vs depth in a ZnSe(200 Å)/GaAs heterostructure shown at 2, 6, and 10 mrad grazing angle, for 9.7 keV energy of incoming photons with s polarization. The solid line represents the result obtained for a heterostructure with no roughness; the dotted line represents the result obtained for a heterostructure with 10 Å of rms roughness.
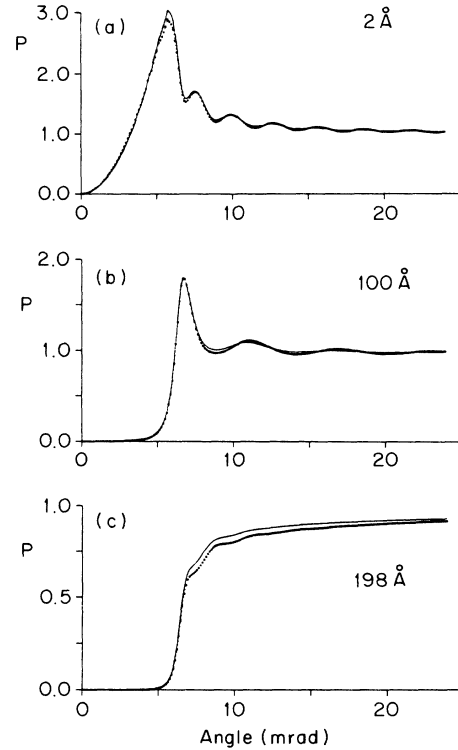
FIG. 4. Calculated magnitude of the normalized Poynting vector vs grazing angle in a ZnSe(200 Å)/GaAs heterostructure shown at depth 2, 100, and 198 Å, for 9.7 keV energy of incoming photons with s polarization. The solid line represents the result obtained for a heterostructure with no roughness; the dotted line represents the result obtained for a heterostructure with 10 Å of rms roughness.

this angular domain. At $z=100$ Å, in the vicinity of the critical angle, the magnitude of the Poynting vector rises rapidly and reaches its maximum, which is about 50% lower than the maximum at $z=2$ Å, and then decreases with some oscillations, whose period is longer than the period of the oscillations at position $z=2$ Å. At $z=198$ Å the magnitude of the energy flow does not exhibit any maximum; instead, it rapidly rises for angles close to the critical angle, and then reaches its limit, which is the magnitude of the incoming energy flow. One can also see weak oscillations. A common feature of these curves is that in the high angle regime they saturate to some constant level below the incoming beam intensity. The presence of roughness may enhance the magnitude of energy flow slightly and smear our oscillations in the region above the critical angle. As we will later observe, the oscillations in the magnitude of the density of energy flow are correlated with oscillations in the direction of energy flow. We would like to point out that these oscillations are an interference effect in stratified media.

In LSM's the Poynting vector lies in the plane of incidence, but in contrast to bulk materials (for s polarization), the direction of energy flow defined by the angle ϕ_j is in general different from the refraction angle θ_j:

$$\tan\phi_j = \frac{P_{jz}}{P_{jx}} \neq \tan\theta_j = C_j \qquad (19)$$

where C_j is constant for the jth layer.

In Fig. 5 the dependence of the ϕ_j upon z is shown for a ZnSe/GaAs heterostructure along with the refraction angle θ_j, for purposes of comparison. For a small, subcritical grazing angle [2 mrad, Fig. 5(a)] energy flows in an almost constant direction that is very close to the refraction angle (i.e., approximately parallel to the surface) throughout most of the epilayer and then, as expected, a very small portion of radiant energy flows in the direction described by constant value of the refracted angle in the substrate. For the critical grazing angle [6 mrad, Fig. 5(b)] ϕ_j remains constant and slightly smaller than the refraction angle in a depth of 100 Å below the surface, and then gradually arises and reaches the constant value θ_2 in the substrate. A very interesting behavior is visible for grazing angles exceeding the critical angle [10 mrad, Fig. 5(c)]. We observe oscillations of the angle of energy flow with increasing amplitude whose period can be estimated using (17):

$$L = \pi/(k_1 \sin\theta_1) . \tag{20}$$

But, as we see, the average direction of the energy flow is almost in the angle of refraction.

In Fig. 6 the dependence of $\phi_1(z,\theta)$ versus incidence angle is shown for a ZnSe/GaAs heterostructure. As mentioned before, at $z = 2$ Å below the surface the direc-
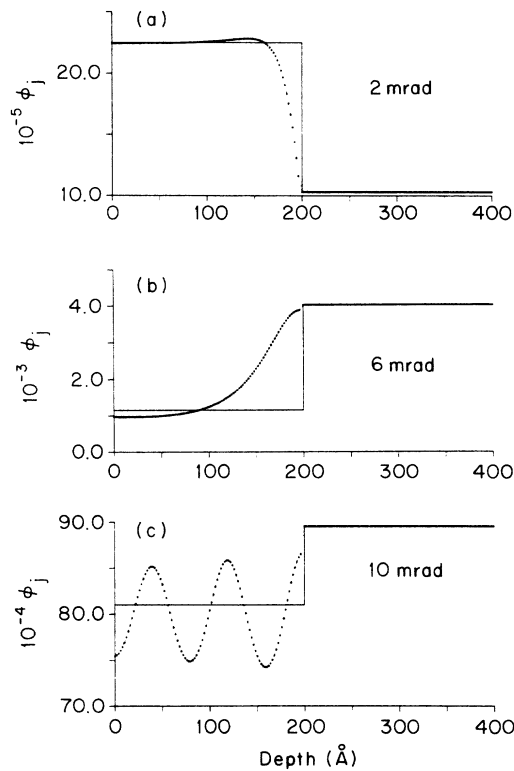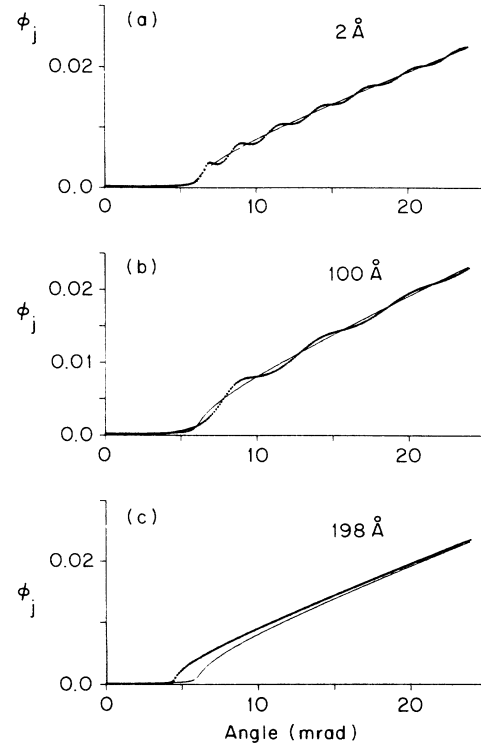

FIG. 6. Comparison of direction of energy flow with direction of real part of wave vector. The dotted line represents the calculated direction of the Poynting vector vs grazing angle in a ZnSe(200 Å)/GaAs heterostructure shown at depth 2, 100, and 198 Å, for 9.7 keV energy of incoming photons with s polarization. The solid line represents the angle of refraction in the ZnSe layer.

FIG. 5. Comparison of direction of energy flow with direction of real part of wave vector. The dotted line represents the calculated direction of the Poynting vector vs depth in a ZnSe(200 Å)/GaAs heterostructure shown at 2, 6, and 10 mrad, for 9.7 keV energy of incoming photons with s polarization. The solid line represents the angle of refraction in the appropriate layer.

tion of energy flow oscillates rapidly around the refraction angle in the domain $\theta > \theta_C$, as expected from (19) [see Fig. 6(a)]. At the midpoint, i.e., at $z = 100$ Å, the direction of energy flow does not oscillate as frequently [see Fig. 6(b)]. In the vicinity of the interface, at $z = 198$ Å [see Fig. 6(c)] it gradually approaches the value of the refraction angle with increasing incidence angle.

The physical situation in superlattices is more involved because the additional appearance of the Bragg standing wave is expected. As an example we will consider a Pt/C×30 LSM with a 5-Å top layer of Hf. Below the critical angle, radiation penetrates a LSM very shallowly [only a few layers, see Figs. 7(a) and 9(a)]; above this angle x-rays penetrate the whole multilayer system [see Figs. 7(b) and 9(b)]. As we can see, the uncorrelated interfacial roughness enhances the density of energy flow (see Figs. 8 and 10). When the Bragg condition on LSM interfaces is fulfilled [see Figs. 7(c) and 9(c)] the Bragg standing wave is observed. The normal component of the density of energy flow is significantly enhanced due to uncorrelated roughness, but the general features of both components are very similar. The parallel components of the density of energy flow obtained for a LSM without roughness oscillate rapidly, with the amplitude decaying relatively quickly, and with well-defined nodal and antinodal planes. The position of these planes is a function of the incidence angle (see Figs. 11 and 12). The presence

of uncorrelated interfacial roughness results in the appearance of a constant level of the density of energy flow in the direction parallel to the interfaces and a decreasing magnitude of oscillations which, however, decay much more slowly than in the case without roughness. We see that the difference between nodal and antinodal planes is not so well defined in the presence of roughness. Although energy density in the antinodal planes close to the surface with roughness is smaller than without it, below some critical thickness this relationship is reversed, which may have important experimental consequences.

B. p polarization

In the case of p polarization the incoming field amplitude E_p can be decomposed into two components: parallel $E_{0x}^+(z_0)$ and perpendicular $E_{0z}^+(z_0)$ to the interface (see Fig. 1), where

$$E_x = E_{0x}^+(z_0) = E_p \sin\theta ,$$ (21a)

$$E_z = E_{0z}^+(z_0) = -E_p \cos\theta ,$$ (21b)

and the magnetic field has only one component:

$$H_y = H_{0y}^+(z_0) = n_0 E_p / \mu$$ (21c)

where μ is the permeability. We should consider every field component independently. To this end we define appropriate matrices for solving the Fresnel equations for the boundary conditions on interfaces and the perturbation due to scattering as follow:

$$\tilde{I}_{j_\alpha} = \frac{1}{\hat{t}_{j\alpha}} \begin{vmatrix} 1 & \hat{r}_{j\alpha} \\ \hat{r}_{j_\alpha} & 1 \end{vmatrix}$$ (22)

and

$$\tilde{S}_{j\alpha} = \frac{1}{1 - (\hat{r}_{j\alpha})^2} \begin{vmatrix} \hat{e}_j^- - (\hat{r}_{j\alpha})^2 e_j^+ & \hat{r}_{j_\alpha}(\hat{e}_j^+ - \hat{e}_j^-) \\ \hat{r}_{j\alpha}(\hat{e}_j^+ - \hat{e}_j^-) & \hat{e}_j^- - (\hat{r}_{j_\alpha})^2 \hat{e}_j^+ \end{vmatrix}$$ (23)

where $\alpha = x$, z, $\hat{e}_j^+$, and $\hat{e}_j^-$ are defined by (7a) and (7b) and $\hat{r}_{j\alpha}$, $\hat{t}_{j\alpha}$ are the Fresnel coefficients for the α components.[48] The LSM will now be represented by matrices $\tilde{P}_x^{ON}$ or $\tilde{P}_z^{ON}$ in a similar way as in (9a) or (10a). For example, the α component of the total electric field at point $z_{j-1} < z < z_j$ is given by
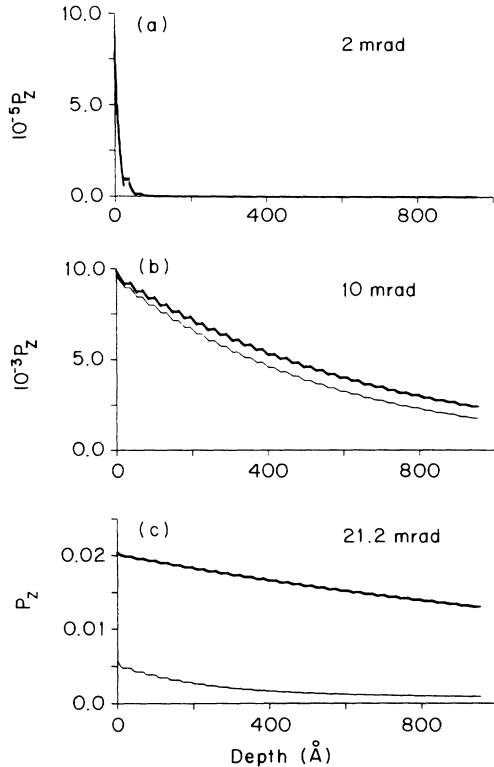

FIG. 7. Calculated magnitude of the normal (z) component of the normalized Poynting vector vs depth in a Hf(5 Å)/{Pt(17.3 Å)/C(14.4 Å)}×30/C superlattice shown at 2, 10, and 21.2 mrad grazing angle, for 9.6 keV energy of incoming photons with s polarization. The thin line represents the result obtained for a superlattice with no roughness; the thick line represents the result obtained for a superlattice with 3 Å of rms roughness. Note that 21.2 mrad is the Bragg angle on the interfaces of this superlattice at that energy.
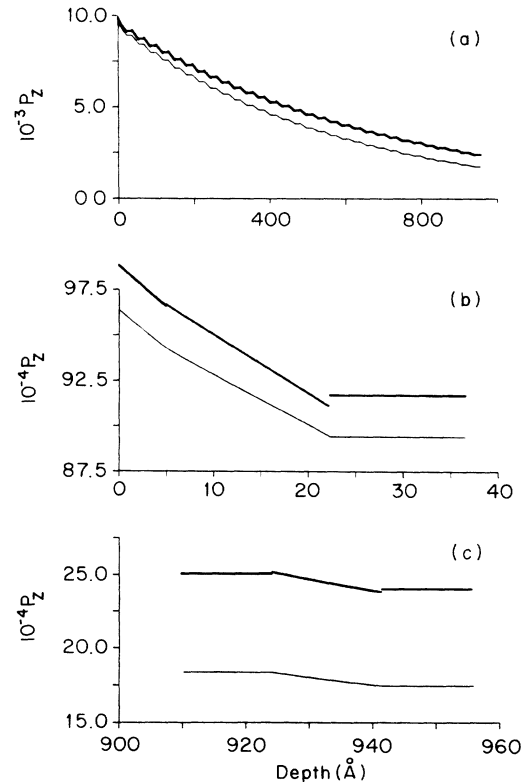

FIG. 8. Calculated magnitude of the normal (z) component of the normalized Poynting vector vs depth in a Hf(5 Å)/{Pt(17.3 Å)/C(14.4 Å)}×30/C superlattice shown at 10 mrad grazing angle, for 9.6 keV energy of incoming photons with s polarization. The thin line represents the result obtained for a superlattice with no roughness; the thick line represents the result obtained for a superlattice with 3 Å of rms roughness. Top: full superlattice; middle: first three layers; bottom: last three layers.

$$E_{j\alpha}(\theta,z) = \{p_{11\alpha}^{jN}\exp[i\hat{p}_j(z_j - z)]$$

$$+ p_{21\alpha}^{jN}\exp[-i\hat{p}_j(z_j - z)]\}E_{0\alpha}^{+}/p_{11\alpha}^{0N} \ .$$

(24)

The magnetic field can be written in the form $(z_{j-1} < z < z_j)$

$$H_j(\theta,z) = [\hat{p}_j(E_{jx}^{+} - E_{jx}^{-}) - k_{0x}(E_{jz}^{+} + E_{jz}^{-})]/k_0$$

$$= H_y(\theta,z) \ .$$

(25)

The time averages of the components of the Poynting vector are

$$P_x(\theta,z) = -C\langle \mathrm{Re}(E_z H_y^*)\rangle \ ,$$

(26a)

$$P_y(\theta,z) = 0 \ ,$$

(26b)

$$P_z(\theta,z) = C\langle \mathrm{Re}(E_x H_y^*)\rangle \ .$$

(26c)

Also in this case energy flows in the plane of incidence and we have $(z_{j-1} < z < z_j)$

$$P_x(\theta,z) = -C\langle \mathrm{Re}\{(E_{jz}^{+} + E_{jz}^{-})[\hat{p}_j^*(E_{jx}^{+*} - E_{jx}^{-*}) - k_{0x}(E_{jz}^{+*} + E_{jz}^{-*})]\}/k_0\rangle \ ,$$

(27a)

$$P_z(\theta,z) = C\langle \mathrm{Re}\{(E_{jx}^{+} + E_{jx}^{-})[\hat{p}_j^*(E_{jx}^{+*} - E_{jx}^{-*}) - k_{0x}(E_{jz}^{+*} + E_{jz}^{-*})]\}/k_0\rangle \ .$$

(27b)

In the substrate $(z > z_N)$

$$P_x(\theta,z) = -C\langle \{\mathrm{Re}[E_{Sz}^{+}\hat{p}_S^*(E_{Sx}^{+*})] - \cos\theta \, | E_{Sz}^{+} |^2\}\rangle \ ,$$

(28a)

$$P_z(\theta,z) = C\langle \mathrm{Re}(\hat{p}_S^*) \, | E_{Sx}^{+} |^2/k_0 - \cos\theta \mathrm{Re}(E_{Sx}^{+}E_{Sz}^{+*})\rangle \ .$$

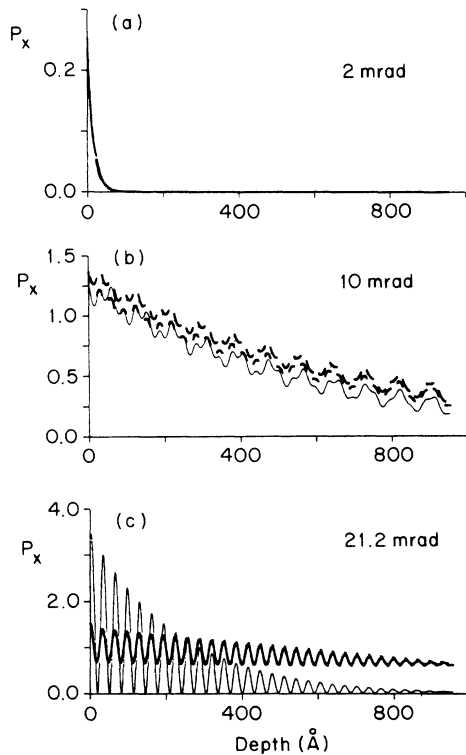(28b)

In the hard x-ray regime and at a grazing angle of in-

FIG. 9. Calculated magnitude of the tangential (x) component of the normalized Poynting vector vs depth in a Hf(5 Å)/{Pt(17.3 Å)/C(14.4 Å)}×30/C superlattice shown at 2, 10, and 21.2 mrad grazing angle, for 9.6 keV energy of incoming photons with s polarization. The thin line represents the result obtained for a superlattice with no roughness; the thick line represents the result obtained for a superlattice with 3 Å of rms roughness. Note that 21.2 mrad is the Bragg angle on the interfaces of this superlattice at that energy.
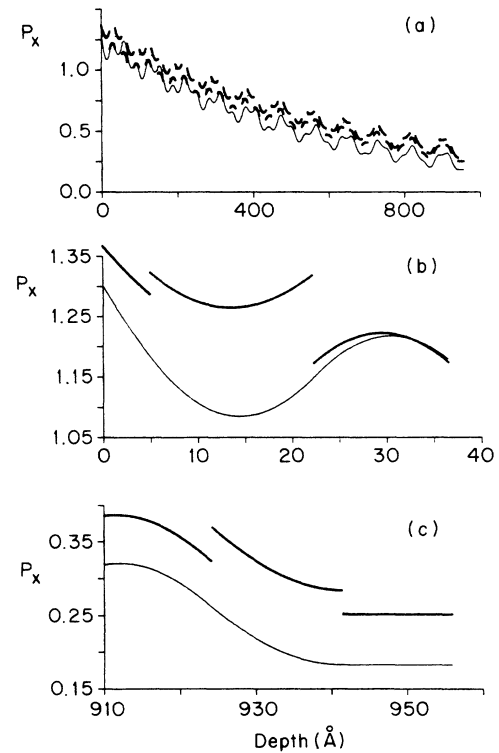

FIG. 10. Calculated magnitude of the tangential (x) component of the normalized Poynting vector vs depth in a Hf(5 Å)/{Pt(17.3 Å)/C(14.4 Å)}×30/C superlattice shown at 10 mrad grazing angle, for 9.6 keV energy of incoming photons with s polarization. The thin line represents the result obtained for a superlattice with no roughness; the thick line represents the result obtained for a superlattice with 3 Å of rms roughness. Top: full superlattice; middle: first three layers; bottom: last three layers.
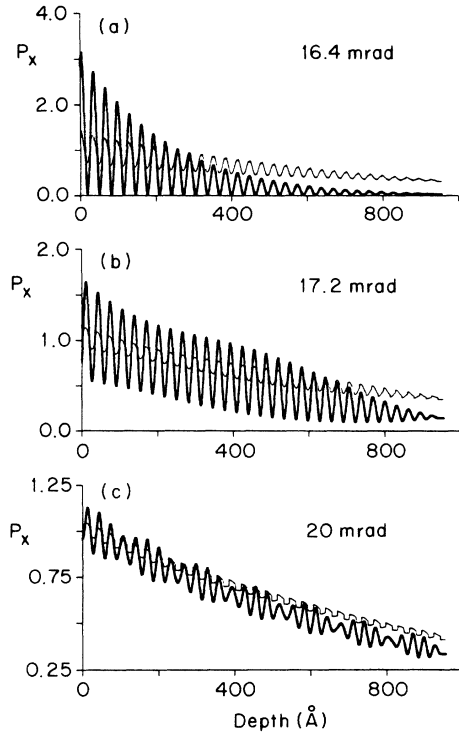
FIG. 11. Calculated magnitude of the tangential (x) component of the normalized Poynting vector vs depth in a $\mathrm{Hf}(5$ Å$)/\{\mathrm{Pt}(17.3$ Å$)/\mathrm{C}(14.4$ Å$)\} \times 30/\mathrm{C}$ superlattice shown at 16.4, 17.2, and 20 mrad grazing angle, for 12 keV energy of incoming photons with s polarization. The thick line represents the result obtained for a superlattice with no roughness; the thin line represents the result obtained for a superlattice with 3 Å of rms roughness. Note that 16.4 mrad is the Bragg angle on the interfaces of this superlattice at that energy.

FIG. 12. Calculated magnitude of the tangential (x) component of the normalized Poynting vector vs depth (z) in the first three layers of a $\mathrm{Hf}(5$ Å$)/\{\mathrm{Pt}(17.3$ Å$)/\mathrm{C}(14.4$ Å$)\} \times 30/\mathrm{C}$ superlattice shown at 16.4, 17.2, and 20 mrad grazing angle, for 12 keV energy of incoming photons with s polarization. The dotted line represents the result obtained for a superlattice with no roughness; the thin line represents the result obtained for a superlattice with 3 Å of rms roughness. Note positions of nodal and antinodal planes.

In the hard x-ray regime and at a grazing angle of incidence the calculated and observed differences between s and p polarization are smaller than 1% for most of the materials. For this reason we will not consider the transverse magnetic wave (TM) mode separately.

C. Mixed case

In the general case the electric and the magnetic fields of incoming radiation can be decomposed into three orthogonal nonvanishing components. As a consequence one should expect that the Poynting vector does not lie in the plane of incidence (cf. Ref. 47). However, the deviation from the plane of incidence for hard x-rays is so small that in most practical cases it can be neglected.

V. FLUORESCENCE YIELD IN LSM WITH INTERFACIAL ROUGHNESS

A. Formulation of the problem

If the incoming photons are energetic enough to fluoresce atoms in the LSM, the angular fluorescence yield will depend on the energy flow at the fluorescent atoms, the dynamical absorption, and the concentration of the atoms. In other words, the fluorescence yield of
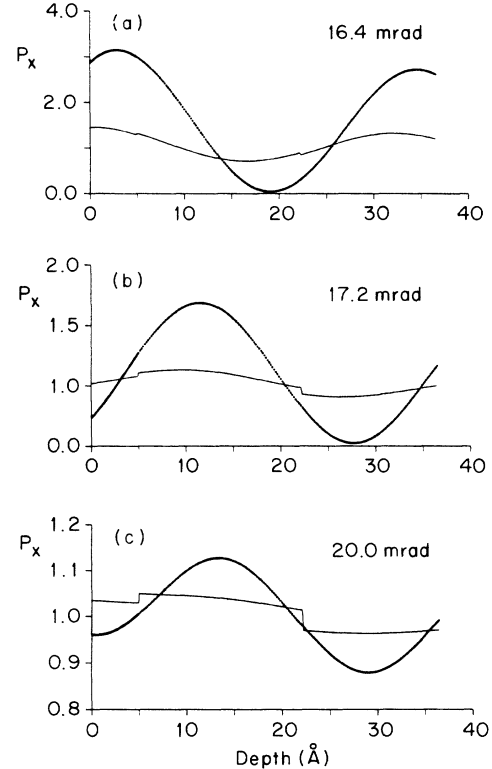
atoms is proportional to the energy loss per unit length, i.e., in the direction normal to the interfaces of stratified media. In our model we will neglect the angular dependence of energy losses due to the Compton effect, phonon scattering, higher shell fluorescence, self-absorption, and other processes. This means we assume that the same portion of absorbed radiant energy is converted into fluorescence emission which in turn does not suffer self-absorption or scattering on its way to an external detector.

Let us consider a rectangular wave front of the incoming radiation with width w_{0i} and of unit height (in the direction perpendicular to the plane of incidence). We can find the time average of the total radiant flux of the incoming beam (F_{i0}), the reflected beam (F_{r0}), and the refracted beam (F_1) at the LSM surface $(z = z_0)$:

$$F_{i0}(\theta,z) = w_{0i}(z_0)P_i(\theta,z) , \tag{29a}$$

$$F_{r0}(\theta,z) = w_{0r}(z_0)P_r(\theta,z) , \tag{29b}$$

$$F_1(\theta,z) = w_1(z_0)P_1(\theta,z) , \tag{29c}$$

where P_i, P_r, and P_1 are the time average of the density of energy flow in the incoming, reflected, and refracted

wave, respectively. We will assume that, for grazing incidence, the width w_j of a wave front in the jth layer is constant. One can easily derive the following formula:

$$w_j = w_{0I} \prod_{k=0}^{j-1} \frac{\sin[\phi_{k+1}(z_k)]}{\sin[\phi_k(z_k)]} \tag{30}$$

where the angles $\phi_{k+1}(z_k)$ and $\phi_k(z_k)$, defined in (19), describe the direction of energy flow at the point z_k in the $(k+1)$th and kth layers, respectively.

Now we are in a position to calculate the angular fluorescence yield (FY), normalized to the incoming flux, from the LSM region between $z=0$ and $z < z_{j-1}$:

$$Y(\theta) = C \frac{F_{i0} - F_{r0} - F_J}{F_{i0}} = C \left[1 - R - \frac{F_j}{F_{i0}} \right]$$

$$= C \left[1 - R - \prod_{k=0}^{j-1} \frac{\sin[\phi_{k+1}(z_k)]}{\sin[\phi_k(z_k)]} \frac{P_j(\theta,z)}{P_{i0}(\theta,z)} \right]$$

$$\tag{31}$$

where R is the reflection coefficient and C is a multiplicative constant.

An obvious consequence of this model is that fluorescence from a homogeneous bulk sample is expected to be the simple complement of the total external reflectivity curve. In the following paragraphs we will consider FY in the evanescent- and standing-wave domains.

B. Evanescent- and standing-wave fluorescence from LSM's

As an example let us analyze the angular FY from a ZnSe/GaAs heterostructure with different layer thicknesses of ZnSe as is predicted by our model [shown in Figs. 13(a) and 13(b)]. For an extremely thin layer (5 Å) FY arises almost linearly with incidence angle, and then reaches a broad maximum at the critical angle, after which it gradually decreases to some small value. With increasing thickness the maximum in FY increases its height and slightly shifts towards a higher angle. Its half-width decreases, reaches its minimum for a layer about 250 Å thick, and increases again for thicker layers. The OEMF model predicts the appearance of oscillations on the high angle side of these maxima. The period of these oscillations is inversely proportional to the layer thickness and their amplitude decays with increasing angle. At very high angles all these curves reach some constant level which increases with layer thickness. The general shape of the FY curve changes for thicker layers [see Fig. 13(b)], the maximum becomes broader, and in the limit of infinite thickness we expect this curve to be the complement of reflectivity for a bulk sample.

The influence of uncorrelated roughness on angular fluorescence emission from a ZnSe/GaAs heterostructure is shown in Figs. 14(a) and 14(b). As expected, increasing the surface rms roughness results in a change of the shape of the FY curve in the subcritical domain (evanescent wave). The FY is now enhanced and this enhancement reaches its maximum at the critical angle. Above the critical angle the enhancement rapidly decreases and is negligible at twice the critical angle. In the standing-
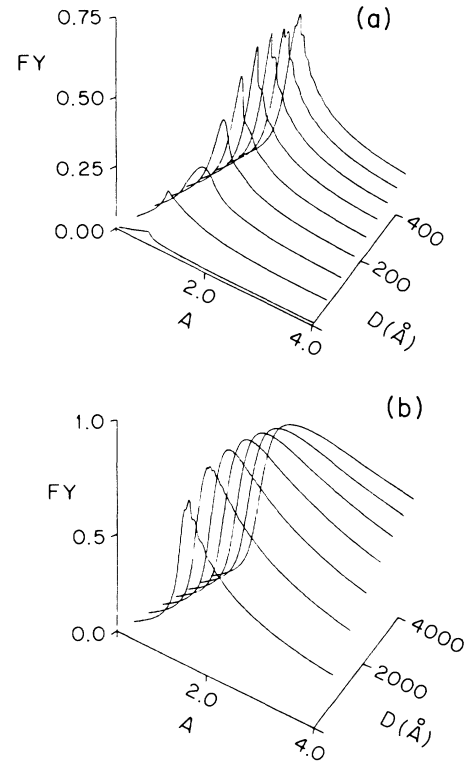

FIG. 13. Calculated normalized fluorescence yield (FY) from the ZnSe layer of a ZnSe/GaAs heterostructure vs normalized grazing angle ($A = \theta/\theta_C$) using ZnSe layer thickness D as a parameter for each FY plot; (a) from 5 through 400 Å, for incidence radiation energy 9.7 keV with s polarization and (b) from 400 through 2800 Å, for incidence radiation energy 9.7 keV with s polarization.

wave region the presence of surface roughness affects the amplitude of FY oscillations and as a result the oscillations become less pronounced.

Obviously the interfacial roughness does not affect evanescent FY. Above the critical angle the presence of roughness lowers the average magnitude of FY and extinguishes the amplitude of its oscillations. The influence of interfacial roughness is significant even at three times the critical angle but is decreasing along increasing incidence angle. The influence of this "perturbation" on FY is strongest for an incidence angle slightly above the critical angle but is an order of magnitude weaker than the effect of surface roughness at its maximum.

In Figs. 15(a) and 15(b) angular FY from a Hf/(Pt/C)×30 LSM predicted by OEMF theory, with various roughness parameter values, is shown. The evanescent portion of the FY curve from the 5-Å Hf top layer [see Fig. 15(a)] increases almost linearly with grazing angle as is expected from the angular dependence of the magnitude of the Poynting vector in a thin layer [see Fig. 4(a)]. The FY from the Pt layers [see Fig. 15(b)] rises sharply in the vicinity of the critical angle, which resembles the behavior of the Poynting vector in a thicker layer [see Figs. 4(b) and 4(c)]. The Hf FY exhibits a maximum at the critical angle, as is expected from our previous analysis, and exhibits almost the same shape of angular
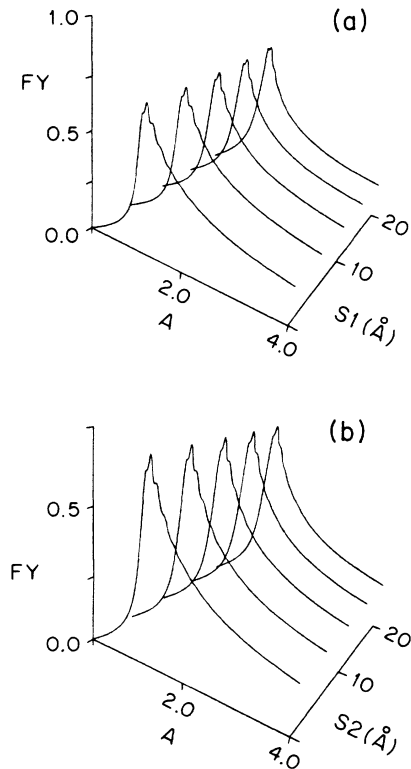
FIG. 14. (a) Calculated normalized fluorescence yield from the ZnSe layer of a ZnSe/GaAs heterostructure vs normalized grazing angle ($A = \theta/\theta_C$) using surface rms roughness (denoted S_1) as a parameter for each FY plot; from 0 through 20 Å, for radiation energy 9.7 keV with s polarization. (b) Same as for (a), but using interfacial rms roughness (denoted S_2) as a parameter for each FY plot; from 0 through 20 Å, for radiation energy 9.7 keV with s polarization.

and 12(a)], at an angle which coincides with the first Bragg reflection peak, then a minimum of fluorescence from these layers is expected [Fig. 15(b)]. On the other hand, if the antinodal planes are in the Pt layers [$\theta = 17.2$ mrad, see Figs. 11(b) and 12(b)] one should expect a maximum in the Pt FY [Fig. 15(b)]. However, as was mentioned before, surface and interfacial roughness diminishes the difference between the magnitude of the nodal and antinodal planes of energy flow. Consequently, the predicted minimum in the FY curve becomes shallower and the maximum is smaller, with the increasing of the rms roughness parameter. Similar behavior in the FY from the top thin layer of Hf is expected [see Fig. 15(a)]. However, in this case of OEMF theory predicts the appearance of an antinodal energy flow plane in the Hf layer [$\theta = 21.2$ mrad, see Fig. 9(c)], i.e., a maximum of Hf FY at the first Bragg reflection peak, and nodal plane, i.e., a minimum at a slightly higher angle. This coincidence between angular position of the first Bragg reflection peak and antinodal plane in the HF layer versus nodal planes in Pt layers results in weakening the
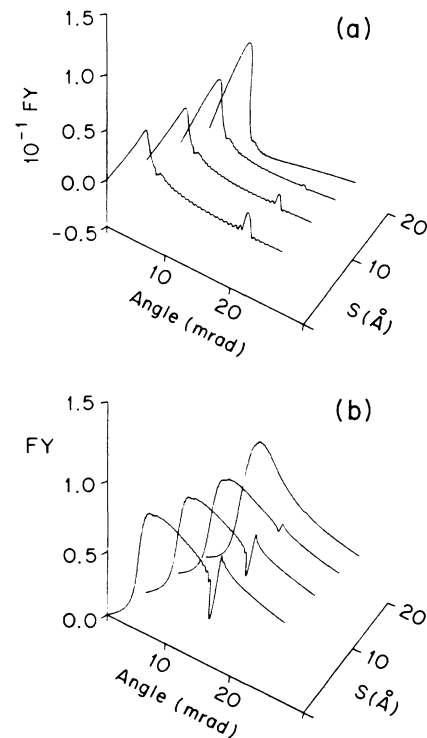
FY as from ZnSe/GaAs heterostructure with a 5 Å thin layer [see Fig. 13(a)] although it is modified by some features due to multilayer effects: high-frequency weak oscillations and Bragg peaks. As expected, the FY from the Pt layers resembles that obtained from a very thick layer of ZnSe [see Fig. 13(b)] in a ZnSe/GaAs heterostructure, but with some superimposed structure due to the above-mentioned superlattice effects.

In order to analyze the influence of uncorrelated roughness on FY from the system, we calculated fluorescence emission from the LSM with different roughness parameters [see Figs. 15(a) and 15(b)]. For simplicity, in the calculation we assumed that for all interfaces the rms roughness parameters are the same. We do observe the same pattern in the influence of roughness on the evanescent- and standing-wave portion of the FY from the superlattice as from the heterostructure. The subcritical domain of the curve is enhanced due to surface roughness while the above-critical domain is diminished due to interfacial roughness. The amplitude of the oscillations in the FY is also diminished due to roughness.

When the Bragg diffraction condition on the LSM interfaces is fulfilled, a very interesting behavior in the angular FY is expected. If the nodal planes of the Poynting vector are in the Pt layers [$\theta = 16.4$ mrad, see Figs. 11(a)

FIG. 15. (a) Calculated normalized fluorescence yield from the Hf layer of a Hf(5 Å)/{Pt(17.3 Å)/C(14.4 Å)}×30/C superlattice vs grazing angle using surface and interfacial rms roughness (denoted S), as a parameter for each FY plot; from 0 through 15 Å, for incidence radiation energy 9.6 keV with s polarization. The maximum at $A = 21.2$ mrad is due to the antinode of a Bragg standing wave in the Hf layer. (b) Calculated normalized fluorescence yield from the Pt layers of a Hf(5 Å)/{Pt(17.3 Å)/C(14.4 Å)}×30/C superlattice vs grazing angle using surface and interfacial rms roughness (denoted S), as a parameter for each FY plot; from 0 through 15 Å, for incidence radiation energy 12.0 keV. The maximum at $A = 17.2$ mrad is due to the antinode of a Bragg standing wave in the Pt layers.

Bragg-diffraction-related maximum on the Hf FY curve versus Pt FY.

The Bragg standing-wave fluorescence from a LSM is also strongly influenced by layer thickness fluctuations. A Debye-Waller-like factor is usually used to describe the effect of this imperfection on reflectivity. The influence of this "perturbation" on LSM reflectivity was studied by Spiller and Rosenbluth.[49] By means of OEMF theory in its recursive version they obtained a reduction of the Bragg peak reflectivity and an enhancement of the reflectivity between them. This in turn will smear out Bragg-related features on the FY curve; however, it should not affect the general shape of angular fluorescence emission from LSM's.

Another important factor which can affect FY from a LSM is the macroscopic surface-substrate slope error (see discussion in Refs. 40 and 41). As a result of this error, the angle of incidence is only well defined locally and one should expect broadening of the maxima in FY with a width roughly proportional to the slope error magnitude. The effect of this perturbation is similar to the effect of the divergence of the incident radiation.

C. Experimental examples

The x-ray experiments were performed at the Cornell High Energy Synchrotron Source at the C-2 station. The sample was positioned on a goniometer driven by stepping motors with 0.01 mrad angular resolution. A two-crystal Si(111) monochromator with very narrow slits was used in order to provide highly collimated and monochromatized radiation. The intensities of the incoming and scattered beams were measured using ion chambers while the fluorescence emission was detected using scintillation counters equipped with filters.

The samples studied were ZnSe/GaAs heterostructures obtained by the MBE method.[50] The measured fluorescence signal is shown in Fig. 16. By fitting the experimental Zn angular FY curve, excited by radiation with 9.7 keV energy (shown in Fig. 16), we concluded that in

this ZnSe/GaAs heterostructure the top roughness parameter is 10 ± 5 Å and the interfacial roughness parameter is 25 ± 5 Å. The high value of interfacial roughness prevents us from detecting oscillations in the angular region above critical angle. These independently found rms roughness parameters are consistent with those obtained from total external reflectivity measurements.[50]

In order to verify the proposed OEMF model, we reinvestigated experimental angular fluorescence yield of Hf and Pt in $Hf/(Pt/C)\times30/C$ LSM obtained by Barbee and Warburton.[40,41] The result is shown in Figs. 17 and 18. By fitting the experimental curves we estimated surface and interfacial rms roughness parameters to be 3 ± 1 and 7 ± 1 Å, respectively. We conclude that incorporation of uncorrelated interfacial roughness into the OEMF model improved significantly the quality of the fit, especially at the Bragg diffraction angle. The weak oscillations in FY predicted by the OEMF theory are apparently below the resolution of the experiment.

VI. CONCLUSIONS

Although only a few experimental examples were analyzed in this paper, we have demonstrated the feasibility of grazing-angle fluorescence as a nondestructive experimental method for the investigation of surface and interfacial roughness and other imperfections in layered synthetic materials. This method is especially suitable for studies of imperfections in thin surface layers since the position of maximum energy flow can be controlled by the incidence angle, and the escaping fluorescence emission does not suffer significant self-absorption. Another virtue of this method is its element sensitivity which in some cases allows us to focus our attention on some selected layers within the LSM.

We proposed the relatively simple OEMF matrix model for calculating the angular x-ray fluorescence from a LSM with uncorrelated interfacial roughness. The model is suitable for both crystalline and amorphous layer struc-
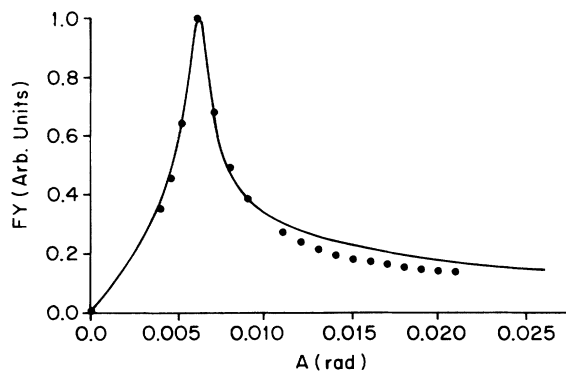

FIG. 16. Comparison of experimental normalized fluorescence yield with calculation based on the model proposed in this paper for a ZnSe(200 Å)/GaAs heterostructure at incident photon energy above the Zn absorption K edge (9.7 keV, s polarization). Dots: experiment; line: calculation based on Eq. (31) with surface and interfacial rms roughness equal to 10 and 25 Å, respectively.
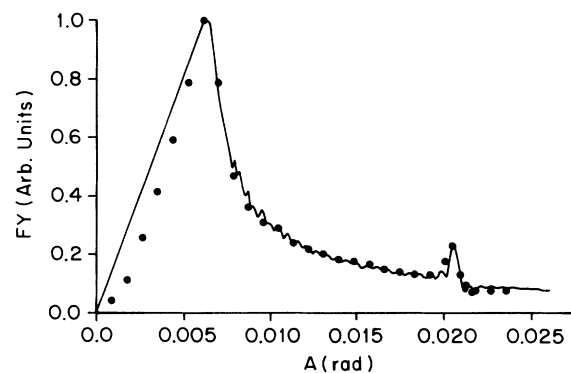

FIG. 17. Comparison of experimental normalized fluorescence yield obtained by Barbee and Warburton (Refs. 40 and 41) with calculation based on the model proposed in this paper for a $Hf(5 \text{ Å})/\{Pt(17.3 \text{ Å})/C(14.4 \text{ Å})\}\times30/C$ superlattice at incident photon energy above the Hf absorption L_{III} edge (9.6 keV). Dots: experiment; line: calculation based on Eq. (31) with surface and interfacial rms roughness equal to 3 and 7 Å, respectively.
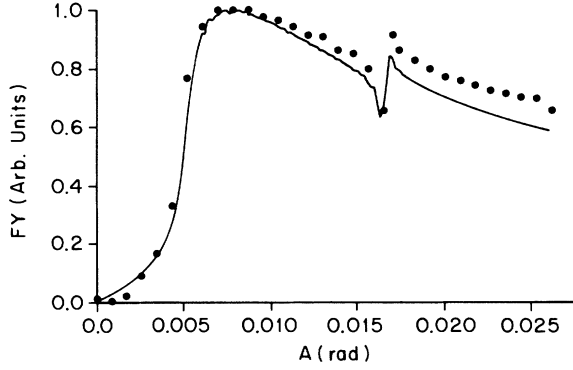
FIG. 18. Comparison of experimental normalized fluorescence yield obtained by Barbee and Warburton (Refs. 40 and 41) with calculation based on the model proposed in this paper for a Hf(5 Å)/{Pt(17.3 Å)/C(14.4 Å)} × 30/C superlattice at incident photon energy above the Pt absorption L_{III} edge (12.0 keV). Dots: experiment; line: calculation based on Eq. (31) with surface and interfacial rms roughness equal to 3 and 7 Å, respectively.

ture. The OEMF model provides us with information on radiant energy flow in the LSM. It can also be used for the calculation of specular reflectivity and transmissivity in stratified media, and can be easily extended to describe other imperfections, such as layer thickness fluctuations, bulk inhomogeneities, slope errors, etc.

ACKNOWLEDGMENTS

APPENDIX

The total electric field $E_j(\mathbf{r})$ in the jth layer of stratified media is

$$E_j(\mathbf{r})=E_j^+(\mathbf{r})+E_j^-(\mathbf{r}) \tag{A1}$$

where

$$E_j^+(\mathbf{r})=\hat{A}_j\exp(i\hat{\mathbf{k}}_j^+\cdot\mathbf{r}) , \tag{A2a}$$

$$E_j^-(\mathbf{r})=\hat{B}_j\exp(i\hat{\mathbf{k}}_j^-\cdot\mathbf{r}) . \tag{A2b}$$

$\hat{\mathbf{k}}_j^+$ and $\hat{\mathbf{k}}_j^-$ are the complex wave vectors for the transmitted and reflected field, respectively. $\hat{A}_j$ and $\hat{B}_j$ are the complex amplitudes

$$\hat{A}_j= | \hat{A}_j | \exp(i\alpha_j) , \tag{A3a}$$

$$\hat{B}_j= | \hat{B}_j | \exp(i\beta_j) . \tag{A3b}$$

In the $(j + 1)$th layer, which is located below the jth interface, the total electric field is as

$$E_{j+1}(\mathbf{r})=E_{j+1}^+(\mathbf{r})+E_{j+1}^-(\mathbf{r}) \tag{A4}$$

where

$$E_{j+1}^+(\mathbf{r})= \hat{A}_{j+1}\exp(i\hat{\mathbf{k}}_{j+1}^+\cdot\mathbf{r}) , \tag{A5a}$$

$$E_{j+1}^-(\mathbf{r})=\hat{B}_{j+1}\exp(i\hat{\mathbf{k}}_{j+1}^-\cdot\mathbf{r}) . \tag{A5b}$$

The electric field in a LSM is an homogeneous plane wave[46,47] with a complex wave vector, which can be written in the following form:[48]

$$\hat{\mathbf{k}}_j^+ =\mathbf{k}_j^+ +i\mathbf{a}_j^+ , \tag{A6a}$$

$$\hat{\mathbf{k}}_j^- =\mathbf{k}_j^- +i\mathbf{a}_j^- , \tag{A6b}$$

where $\mathbf{k}_j^-,\mathbf{k}_j^+$ are the real wave vectors defining planes of constant phase for the reflected and transmitted components, respectively. $\mathbf{a}_j^-$ and $\mathbf{a}_j^+$ are real attenuation vectors defining planes of constant amplitude. It can be easily proven[48] that the following equation holds for both the $-$ and $+$ components:

$$\hat{k}_j^2=k_0^2\hat{n}_j^2 \tag{A7}$$

or in terms of its real and imaginary parts:

$$k_j^2-a_j^2=k_0^2[(1-\delta_j)^2-\beta_j^2] , \tag{A8a}$$

$$\mathbf{k}_j\cdot\mathbf{a}_j=k_0(1-\delta_j)\beta_j , \tag{A8b}$$

where $k_0=2\pi/\lambda$ and λ is the wavelength of the incoming radiation in vacuum.

One can obtain from the boundary conditions that $\mathbf{k}_j$ and $\mathbf{k}_{j+1}$ are coplanar and lie in the plane of incidence. The boundary conditions also imply that $\mathbf{a}_j$ and $\mathbf{a}_{j+1}$ are perpendicular to the interfaces, which means that planes of constant amplitude are parallel to the interface. In vacuum (or air) $\beta_0=0$ and the reflected field is a homogeneous plane wave, hence

$$k_j= | \mathbf{k}_j^+ | = | \mathbf{k}_j^- | , \tag{A9a}$$

$$a_j= | \mathbf{a}_j^+ | = | \mathbf{a}_j^- | , \tag{A9b}$$

$$\theta_j=\theta_j^+=\theta_j^- . \tag{A9c}$$

One can also obtain formulas (3c) and (3d):

$$k_{jx}=k_j\cos\theta_j=k_{j+1}\cos\theta_{j+1}=k_{j+1x}=k_{0x} , \tag{A9d}$$

$$\hat{p}_j=k_j\sin\theta_j+ia_j=(k_0^2\hat{n}_j^2-k_0^2n_0^2\cos^2\theta)^{1/2} , \tag{A9e}$$

where θ_j is the angle between the plane of constant phase and the interface in the medium j. θ is the grazing angle of incidence. From the formulas (A2a), (A2b), (A5a), and (A5b) we have (3a) and (3b):

$$E_j^+(\mathbf{r})= \hat{A}_j\exp(i\hat{p}_jz)\exp(ik_{0x}x) , \tag{A10a}$$

$$E_j^-(\mathbf{r})=\hat{B}_j\exp(-i\hat{p}_jz)\exp(ik_{0x}x) . \tag{A10b}$$

[1]H. A. Compton and S. K. Alison, *X-Rays in Theory and Experiment* (Van Nostrand, New York, 1935).

[2]R. W. James, *The Optical Principles of the Diffraction of X-Rays* (Cornell University Press, Ithaca, 1965).

[3]B. W. Batterman and H. Cole, Rev. Mod. Phys. **36**, 681 (1964).

[4]G. H. Vineyard, Phys. Rev. B **26**, 4146 (1982).

[5]D. Litman and I. Sebelova, Opt. Acta **32**, 839 (1985).

[6]B. L. Hanke, J. Y. Uejio, H. T. Yamada, and R. E. Tackaberry, Opt. Eng. **32**, 959 (1986).

[7]M. Born and E. Wolf, *Principles of Optics* (Pergamon, New York, 1965).

[8]P. H. Berning, Phys. Thin Films **1**, 69 (1963).

[9]G. B. Airy, Philos. Mag. **2**, 20 (1933).

[10]H. Kiessing, Ann. Phys. (NY) **5**, 715 (1931); **5**, 765 (1931).

[11]L. G. Parratt, Phys. Rev. **35**, 359 (1954).

[12]T. W. Barbee, Opt. Eng. **25**, 898 (1986).

[13]O. J. Peterson, J. M. Thorne, L. V. Knight, and T. W. Barbee, Proc. Soc. Photo-Opt. Instrum. Eng. **447**, 27 (1981).

[14]J. M. Eastman, Ph.D. thesis, University of Rochester, 1974; Phys. Thin Films **10**, 167 (1978).

[15]P. Beckmann and A. Spizzichino, *The Scattering of Electromagnetic Waves from Rough Surfaces* (Pergamon, New York, 1963).

[16]J. M. Elson and J. M. Bennett, J. Opt. Soc. Am. **69**, 31 (1979).

[17]C. K. Carniglia, Opt. Eng. **18**, 104 (1979).

[18]M. L. Scott and J. M. Elson, Appl. Phys. Lett. **32**, 158 (1978); J. M. Elson, J. Opt. Soc. Am. **69**, 48 (1979); J. M. Elson, J. P. Rahn, and J. M. Bennett, Appl. Opt. **19**, 669 (1980); **16**, 2873 (1977).

[19]P. Croce, J. Opt. **10**, 141 (1979).

[20]L. Névot and P. Croce, Appl. Rev. Phys. **15**, 761 (1980).

[21]P. Bousquet, F. Flory, and P. Roche, J. Opt. Soc. Am. **71**, 1115 (1981).

[22]B. Vidal and P. Vincent, Appl. Opt. **23**, 1794 (1984).

[23]A. Roger, Opt. Acta **30**, 575 (1983).

[24]B. W. Batterman, Phys. Rev. **133**, A759 (1964).

[25]B. W. Batterman, Phys. Rev. Lett. **22**, 703 (1969).

[26]J. A. Golovchenko, B. W. Batterman, and W. L. Brown, Phys. Rev. B **10**, 4239 (1974).

[27]P. Trucano, Phys. Rev. B **13**, 2524 (1976).

[28]S. Andersen, J. A. Golovchenko, and G. Mair, Phys. Rev.

Lett. **37**, 1141 (1976).

[29]P. L. Cowan, J. A. Golovchenko, and M. F. Robbins, Phys. Rev. Lett. **44**, 1680 (1980).

[30]J. A. Golovchenko, J. R. Patel, D. R. Kaplan, P. L. Cowan, M. J. Bedzyk, Phys. Rev. Lett. **49**, 560 (1982).

[31]J. R. Patel and J. A. Golovchenko, Phys. Rev. Lett. **50**, 1858 (1983).

[32]G. Materlik, A. Frahm, and M. J. Bedzyk, Phys. Rev. Lett. **52**, 441 (1984).

[33]M. J. Bedzyk and G. Materlik, Phys. Rev. B **31**, 4110 (1985).

[34]G. Materlik, J. Zegenhagen, and W. Uelhoff, Phys. Rev. B **32**, 5502 (1985).

[35]M. J. Bedzyk and G. Materlik, Phys. Rev. B **32**, 6465 (1985).

[36]R. S. Becker, J. A. Golovchenko, and J. R. Patel, Phys. Rev. Lett. **50**, 153 (1983).

[37]A. Iida, K. Sakurai, A. Yoshinaga, and Y. Gohshi, Nucl. Instrum. Methods A **246**, 736 (1986).

[38]P. L. Cowan, S. Brennan, T. Jach, M. J. Benzyk, and G. Matterlik, Phys. Rev. Lett. **57**, 2399 (1986).

[39]J. M. Bloch, M. Sansono, F. Rondaler, D. G. Peiffer, P. Pincus, M. W. Kim, and P. M. Eisenberger, Phys. Rev. Lett. **54**, 1639 (1985).

[40]T. W. Barbee and W. K. Warburton, Mater. Lett. **3**, 17 (1984).

[41]T. W. Barbee, Superlatt. Microstruct. **1**, 311 (1985).

[42]M. J. Bedzyk, D. Bilderback, J. White, H. D. Abruna, and M. G. Bommarito, J. Phys. Chem. **90**, 4926 (1986).

[43]T. Matsushita, A. Iida, T. Ishikawa, T. Nakagiri, and K. Sakai, Nucl. Instrum. Methods A **246**, 751 (1986).

[44]K. Akimoto, T. Ishikawa, T. Takashashi, and S. Kikuta, Nucl. Instrum. Methods A **246**, 755 (1986).

[45]S. K. Sinha, E. B. Sirota, S. Garoff, and H. B. Stanley, Phys. Rev. B **38**, 2297 (1988).

[46]A. Mahan, J. Opt. Soc. Am. **46**, 913 (1956).

[47]M. Lefévère and M. Montel, Opt. Acta **20**, 97 (1973).

[48]J. M. Stone, *Radiation and Optics* (McGraw-Hill, New York, 1963).

[49]E. Spiller and A. E. Rosenbluth, Opt. Eng. **25**, 954 (1986).

[50]A. Król, C. J. Sher, S. C. Woronick, Y. H. Kao, R. J. Dalby, D. A. Commack, and R. N. Bhargava, in Proceedings of the Third International Conference on Superlattices, Microstructures and Microdevices, Chicago (1987).